Identification of robust genetic signatures associated with lipopolysaccharide-induced acute lung injury onset and astaxanthin therapeutic effects by integrative analysis of RNA sequencing data and GEO datasets

Kaimin Mao[1,*], Wei Geng[1,*], Yuhan Liao[1,*], Ping Luo[2], Hua Zhong[3], Pei Ma[1], Juanjuan Xu[1], Shuai Zhang[1], Qi Tan[1], Yang Jin[1]

[1]Department of Respiratory and Critical Care Medicine, NHC Key Laboratory of Pulmonary Diseases, Union Hospital, Tongji Medical College, Huazhong University of Science and Technology, Wuhan 430022, Hubei, China
[2]Center for Translational Medicine, Union Hospital, Tongji Medical College, Huazhong University of Science and Technology, Wuhan 430022, Hubei, China
[3]College of Life Sciences, Wuhan University, Hubei Province, Wuhan 430072, China
*Equal contribution

Correspondence to: Yang Jin; **email:** whuhjy@126.com, https://orcid.org/0000-0003-2409-7073

ABSTRACT

Acute lung injury (ALI) and acute respiratory distress syndrome (ARDS) are life-threatening clinical conditions predominantly arising from uncontrolled inflammatory reactions. It has been found that the administration of astaxanthin (AST) can exert protective effects against lipopolysaccharide (LPS)-induced ALI; however, the robust genetic signatures underlying LPS induction and AST treatment remain obscure. Here we performed a statistical meta-analysis of five publicly available gene expression datasets from LPS-induced ALI mouse models, conducted RNA-sequencing (RNA-seq) to screen differentially expressed genes (DEGs) in response to LPS administration and AST treatment, and integrative analysis to determine robust genetic signatures associated with LPS-induced ALI onset and AST administration. Both the meta-analyses and our experimental data identified a total of 198 DEGs in response to LPS administration, and 11 core DEGs (*Timp1, Ly6i, Cxcl13, Irf7, Cxcl5, Ccl7, Isg15, Saa3, Saa1, Tgtp1,* and *Gbp11*) were identified to be associated with AST therapeutic effects. Further, the 11 core DEGs were verified by quantitative real-time PCR (qRT-PCR) and immunohistochemistry (IHC), and functional enrichment analysis revealed that these genes are primarily associated with neutrophils and chemokines. Collectively, these findings unearthed the robust genetic signatures underlying LPS administration and the molecular targets of AST for ameliorating ALI/ARDS which provide directions for further research.

INTRODUCTION

Acute respiratory distress syndrome (ARDS) is an acute inflammatory lung injury, associated with increased pulmonary vascular permeability, increased lung weight, and loss of aerated lung tissue [1]. Its less severe form is acute lung injury (ALI). Most patients need mechanical ventilation for support. The initial acute or exudative phase of ALI/ARDS is characterized by the rapid onset of dyspnea, hypoxemia, respiratory failure, and bilateral infiltrates on chest radiographs that are consistent with pulmonary edema [2]. ALI/ARDS is common and has been associated with several clinical disorders, such as sepsis; pneumonia; aspiration of gastric contents,

saltwater, or freshwater; major trauma; transfusion of blood products; acute pancreatitis; and drug reactions (for example, reactions to lipopolysaccharide) [3]. In the past 50 years, considerable progress has been made in understanding the epidemiology, pathogenesis, and pathophysiology of ARDS. However, ARDS is being increasingly recognized as a heterogeneous syndrome, generating momentum for the identification of clinical and biological features for classifying patients into sub-phenotypes that might be more responsive to specific therapies.

Lipid A (endotoxin), the hydrophobic anchor of lipopolysaccharide (LPS), is a glucosamine-based phospholipid that makes up the outer monolayer of the outer membranes of most Gram-negative bacteria [4]. In recent years, LPS, which has been most widely used in drug-associated ALI models, can effectively induce a neutrophilic inflammatory response accompanied by an increase in intrapulmonary cytokines. Many studies have shown that oxidative stress plays a major role in the pathogenesis of lung injury in a murine model of ALI induced by lipopolysaccharide (LPS) [5–7]. In response to the increased formation of reactive oxygen species (ROS), thioredoxin interacting protein (TXNIP) detaches from thioredoxin (Trx), binds to the nucleotide-binding domain-like receptor protein 3 (NLRP3), and then activates NLRP3 inflammasome [8]. The activation of the NLRP3 inflammasome results in the maturation and release of pro-inflammatory cytokines, such as interleukin-1β (IL-1β), which further aggravates the production of inflammatory cytokines (tumor necrosis factor-α (TNF-α), IL-6, inducible nitric oxide synthase (iNOS), and cyclooxygenase-2 (COX2)) and induces oxidative stress [9–11].

Astaxanthin (AST) is a lipid-soluble, red-orange-colored xanthophyll carotenoid synthesized by many micro-organisms and various types of marine life. The main producers of natural AST are microalgae and fungi. Aquatic animals such as salmon, red seabream, shrimp, lobster and crayfish, which feed on AST-producing organisms, are significant dietary sources of AST for humans [12–14]. It has been revealed that AST can prevent inflammatory processes by blocking the expression of pro-inflammatory genes as a consequence of suppressing nuclear factor kappaB (NF-κB) activation [15]. Some studies also suggested that AST has a dose-dependent ocular anti-inflammatory effect, through the suppression of NO, PGE2, and TNF-alpha production, which is achieved by directly blocking NOS enzyme activity [16]. Furthermore, AST has great therapeutic value for lung disease, such as an antifibrotic effect against the promotion of myofibroblast apoptosis based on dynamin-related protein-1 (Drp1)-mediated mito-chondrial fission in vivo and in vitro [17] and anti-

inflammatory effect against LPS-induced ALI, as mentioned above [18, 19]. However, at the transcriptional level, the mechanism of action of AST in the treatment of ALI-/ ARDS- remains unclear. Therefore, we hope to explore the molecular targets of AST against ALI- / ARDS- through further research, with the purpose of providing a new alternative for the clinical treatment of this acute lung disease.

RESULTS

Data processing and meta-analysis of the five microarrays

To determine the common molecular signatures underlying LPS-induced mouse ALI initiation, five microarray datasets were obtained from corresponding independent studies. The characteristics of the studies composing the five gene expression compendiums are listed in Table 1 and Supplementary Table 1. We extracted and annotated the five microarrays, which yielded a collection of 4093 unique genes from 64 samples, including 26 control and 36 LPS-induced ALI mice. Before the meta-analysis study, we comprehensively analyzed the five datasets by identifying the differentially expressed genes in each data set and evaluated overlapping significant genes. The overlapping results were used to generate a Venn diagram (Figure 1), and three genes (*Ccl12, Zbp1,* and *Cxcl13*) were identified in the common region, suggesting that these three genes were significantly correlated with LPS management in mice in the five datasets.

Then, we performed a meta-analysis using NetworkAnalyst (http://www.networkanalyst.ca), which is a comprehensive web-based tool designed to perform meta-analyses of gene expression data [20]. An overview outlining the procedure of the analysis is presented in Figure 2A. Using three meta-analysis approaches, namely Fisher's method, Fixed effect model and Voting count, 3139, 2143 and 3223 differentially expressed genes, respectively, were identified. Among these genes, 2097 were identified by all three methods (Figure 2B), with 1043 (49.7%) genes being upregulated and 1054 (50.3%) being downregulated in the LPS group compared with the control group. A full list of the 2097 common genes identified by the three meta-analysis methods is presented in Supplementary Table 2. A heat map of the top 50 common DEGs across the five datasets is displayed in Figure 2C. Of note, the 10 top upregulated genes (P<0.05) were *Junb, Vcam1, Ehd1, Ifrd, Adm, Cd83, Nadk, Litaf, Tubb6,* and *Ctps*. The 2 most significantly downregulated genes (P<0.05) among the top 50 common DEGs were *Acss1* and *Abcd3*. The merged data from this meta-analysis are listed in Supplementary Data 1.

Table 1. Characteristics of studies composing the five gene expression compendium.

| Study	Dataset	Platform	Region	Types of sample	Sample (Control)	Sample (LPS-ALI)
[60]	GSE102016	Affymetrix Mouse Gene 1.1 ST Array	Maastricht, Limburg Netherlands	Mouse lung tissue	3	3
[58]	GSE2411	Affymetrix Mouse Expression 430A Array	Seattle, WA USA	Mouse lung tissue	6	6
[62]	GSE16409	Amersham CodeLink UniSet Mouse 20K I Bioarray	Durham, NC USA	Mouse lung tissue	3	9
[59]	GSE104214	Agilent-028005 SurePrint G3 Mouse GE 8x60K Microarray	New Haven, CT USA	Mouse lung tissue	6	11
[61]	GSE18341	Affymetrix Mouse Genome 430 2.0 Array	Seattle, WA USA	Mouse lung tissue	8	8
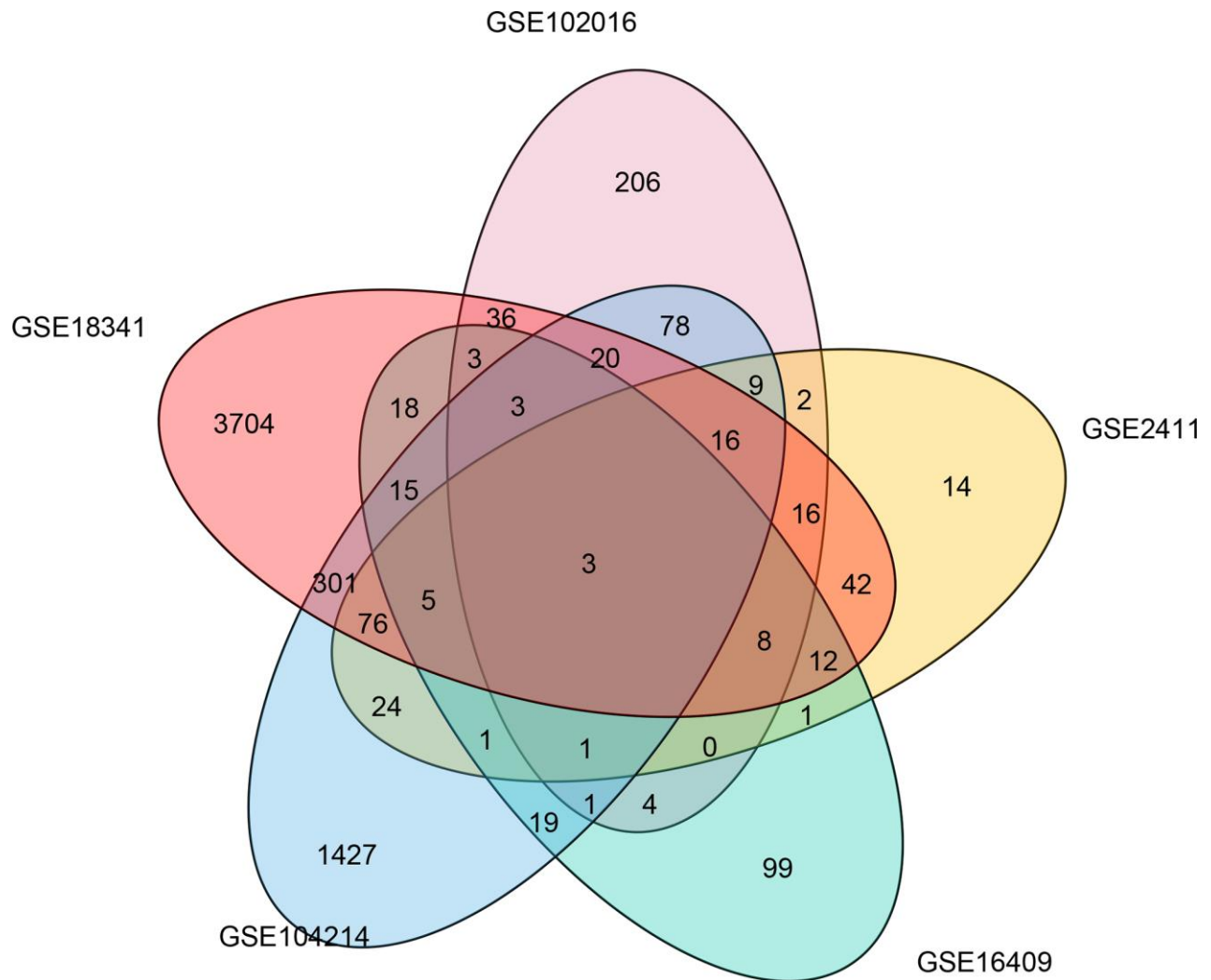
Figure 1. Common differentially expressed genes associated with LPS induction in five microarray studies. A Venn diagram was constructed to show the overlapping differentially expressed genes associated with LPS induction identified in five microarray studies.

Identification of DEGs associated with AST treatments

To further identify the robust expression signatures in LPS-induced ALI and investigate the transcriptional changes resulting from treatment of ALI with AST, we divided mice into three groups, including the control group, LPS group, and AST group. RNA-sequencing (RNA-seq) was performed to profile differentially expressed genes (DEGs) associated with LPS-induced ALI initiation and AST treatment. A total of 1187 DEGs were identified in the LPS-induced ALI group compared with the control group. Among these genes, 989 were
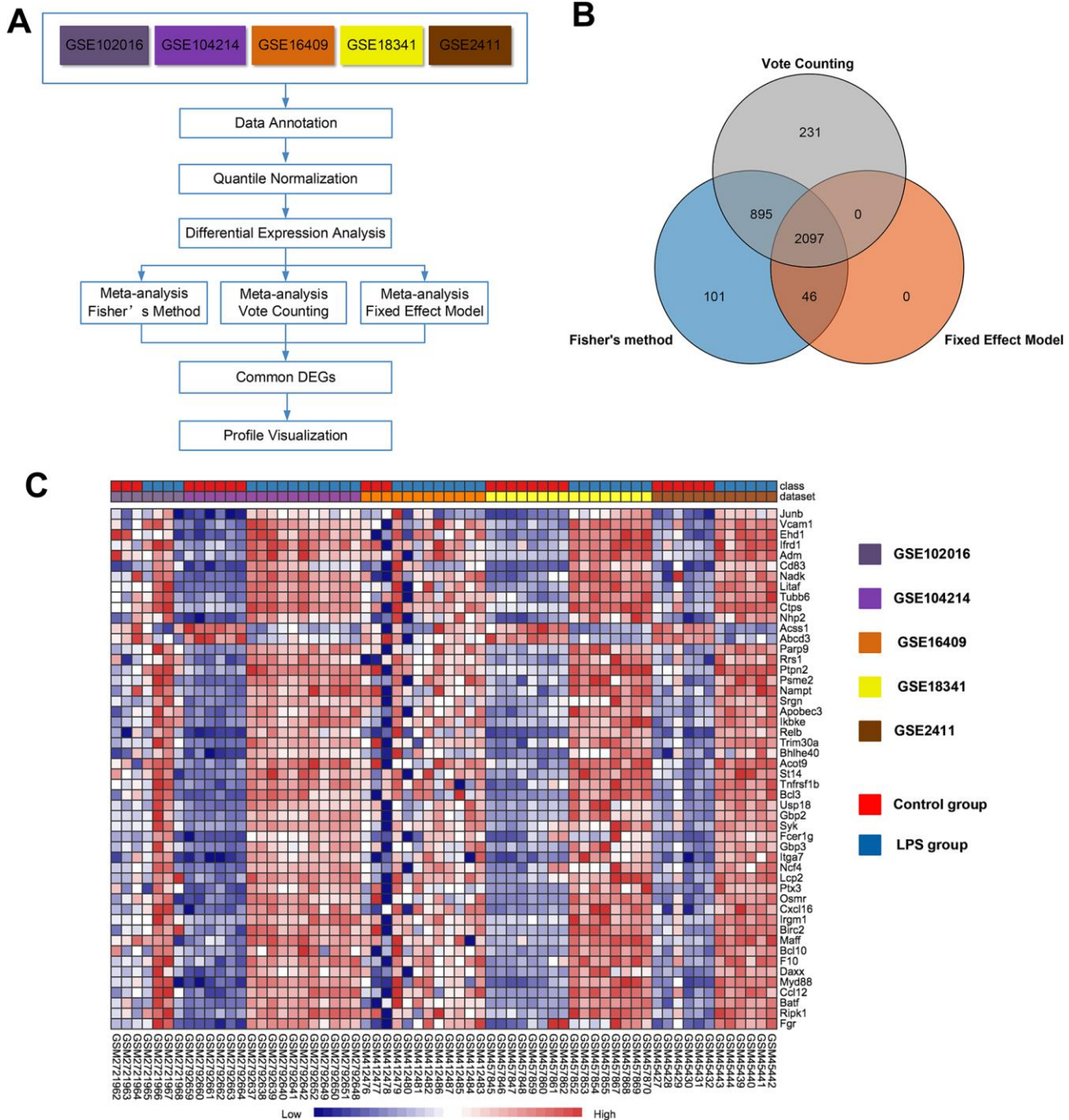

Figure 2. Meta-analysis of five microarrays to identify genes related to LPS induction. (**A**) Flowchart of the meta-analysis approach. (**B**) Venn diagram of differentially expressed genes identified by the meta-analysis using Fisher's method, the vote-counting method, and a fixed-effect model. (**C**) Heat map visualization of the top 50 consistently differentially expressed genes (either completely upregulated or downregulated) across the five microarrays identified by the meta-analysis (row-wise comparison).

significantly upregulated, and 198 were significantly downregulated (Figure 3A and Supplementary Figure 2-1, Supplementary Figure 2-2). A complete list of the differentially expressed genes is provided in

Supplementary Table 3. Then, we compared these genes with the DEGs obtained from the above meta-analysis, and generated two heat- maps of the common DEGs across the meta-analysis results and our experimental
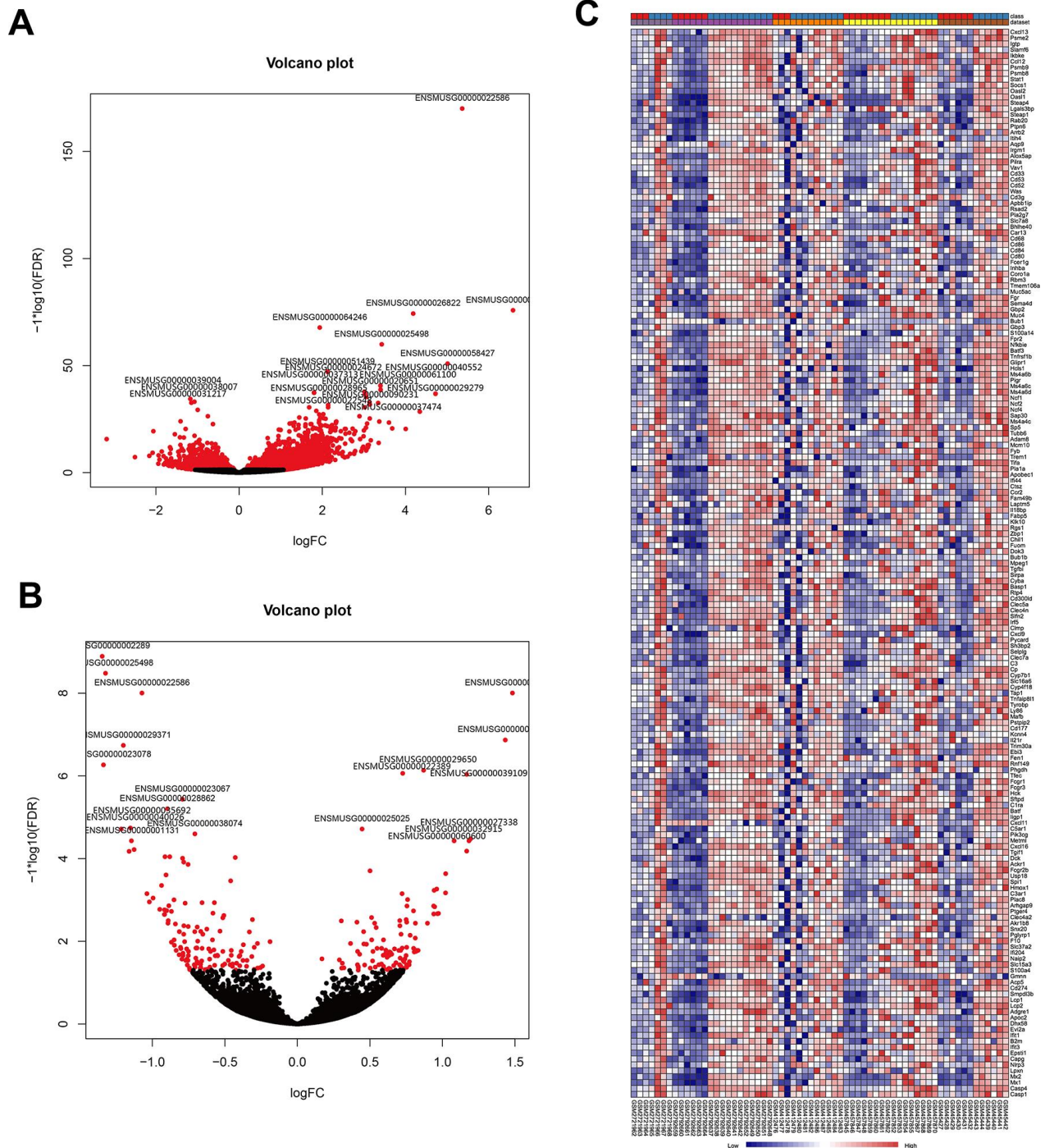

Figure 3. Visualization of DEGs identified by RNA sequencing and the overlap of the results with the meta-analysis of the five microarrays. (**A**) Volcano plot representation of the1187 DEGs associated with LPS-induced ALI onset identify by RNA sequencing (control group vs. LPS group). (**B**) Volcano plot representation of the 21 DEGs associated with the AST therapeutic effect of AST identified by RNA sequencing (LPS group vs. AST group). (**C**) Heat map of the 181 overlapping upregulated genes identified by both meta-analysis of published microarrays and our RNA sequencing experiments (control group vs. LPS group).

data, which are displayed in Figure 3C and Supplementary Figure 1. In total, 198 DEGs were detected in both published data and our experimental data, including 181 upregulated and 17 downregulated DEGs.

To explore the therapeutic effect of AST against ALI at the genetic level, we also compared the gene expression profile of the LPS-induced ALI group with that of the AST treatment group. In total, 21 DEGs were identified after AST treatment (Figure 3B and Supplementary Figure 3-1, and Supplementary Figure 3-2), of which 9 were significantly upregulated and 12 were significantly downregulated (Supplementary Table 4). We subsequently integrated the RNA-seq and microarray meta-analysis data, and 11 core DEGs (*Timp1, Ly6i, Cxcl13, Irf7, Cxcl5, Ccl7, Isg15, Saa3, Saa1, Tgtp1*, and *Gbp11*) that were upregulated in ALI models and downregulated significantly after AST treatment were identified (Table 2).

Functional annotation of core DEGs

To understand the function of the 11 core DEGs, GO enrichment analysis including molecular function (MF), biological process (BP) and cellular component (CC) categories (Supplementary Table 5) was performed using the 'clusterprofile' package in R [21]. In BP terms, the upregulated genes were associated with "cell chemotaxis," the "chemokine−mediated signaling pathway," and "neutrophil migration" (Figure 4A).

Several studies have shown that neutrophil migration and related chemokine network regulation in the lung play roles in the pathogenesis and development of ALI/ARDS [22–24]. In the MF category, the core DEGs were associated with "glycosaminoglycan binding," "chemokine activity," and "receptor-ligand activity" (Figure 4B). Since glycosaminoglycan–cytokine interactions have been reported to support cellular mechanisms that cause acute inflammation [25], AST may affect these interactions by downregulating the genes involved to exert an anti-inflammatory effect. Moreover, DEGs were enriched in the CC category involved in "high−density lipoprotein particles," "symbiont−containing vacuole membranes," and "plasma lipoprotein particles" (Figure 4C).

Validation of core DEGs

To further confirm the differences in the expression of the 11 core DEGs (*Timp1, Ly6i, Cxcl13, Irf7, Cxcl5, Ccl7, Isg15, Saa3, Saa1, Tgtp1*, and *Gbp11*) among the control group, LPS group, and AST group, we divided mice into three groups and conducted qRT-PCR and IHC verification (Figure 5A–5K, Supplementary

Figure 4). The results demonstrate that the relative expression levels of all 11 genes were significantly upregulated in the LPS group compared to the control group. More importantly, the expression levels of the above 11 DEGs, as analyzed by qRT-PCR, were significantly inhibited after the application of AST. Of the 11 core genes, 8 were tested by IHC, and the results were consistent with the qRT-PCR results, which further verifying the data (Supplementary Figure 4). Overall, the RT-qPCR and IHC results were consistent with our integrative RNA-seq analysis and meta-analysis, suggesting the critical role that the 11 core DGEs might play in the mechanism by which AST alleviates ALI/ARDS.

DISCUSSION

As a life-threatening condition, ALI/ARDS is an underrecognized condition, and its treatment is an unmet medical need. It is thought that inflammatory storm is the key factor in the occurrence of ALI [26], and anti-inflammatory and antioxidant therapy should be the primary objective in ALI/ARDS [27]. To find the conserved genes responsible for LPS-induced ALI initiation and the effects of AST treatment, we identified robust changes in gene expression related to ALI by meta-analysis and RNA-seq using the Gene Expression Omnibus (GEO) database and mice, respectively. Moreover, we performed functional enrichment analysis of core genes using the Gene Ontology (GO) database to explore the possible molecular mechanisms that mediate the therapeutic effect of AST. Before the meta-analysis of the five microarray datasets, we compared the differentially expressed genes in each dataset, and 3 common differentially expressed genes (DEGs) were found in all five datasets: *Cxcl13, Zbp1, and Ccl12*. CXCL13 is abnormally expressed in the lung tissues of patients with idiopathic pulmonary fibrosis (IPF), and its circulating concentration is also highly correlated with the clinical manifestations and disease progression of individual patients. In the lung tissues of patients with IPF, CXCL13 may promote focal infiltration of nonproliferating B cells through the CXCL13-CXCR5 axis [28]. ZBP1 is a host protein that was shown to be an innate sensor of viral infection, regulating cell death, inflammasome activation, and proinflammatory responses in a variety of situations, including infection and embryonic development [29]. A previous study indicated that ZBP1 is abnormally expressed in H1N1-induced pneumonia associated with acute respiratory distress syndrome in mice [30]. CCL12 (MCP1), which is elevated in pulmonary fibrosis, has been reported to mediate fibroblast survival through IL-6 [31]. Since fibroproliferation is initiated early in lung injury, it has been observed that CCL12 is highly expressed in ARDS

Table 2. List of eleven core DEGs.

Gene	ENSEMBL ID	AST vs LPS			LPS vs Control		
		log2 Fold Change	P-value	P-adj	log2 Fold Change	P-value	P-adj
Timp1	ENSMUSG00000001131	-1.144380002	4.22E-08	3.74E-05	3.079304599	3.48E-26	1.23E-23
Ly6i	ENSMUSG00000022586	-1.07173215	2.35E-12	9.97E-09	5.366650913	4.43E-175	7.5E-171
Cxcl13	ENSMUSG00000023078	-1.337143037	2.23E-10	5.38E-07	1.311102736	0.000340307	0.002635586
Irf7	ENSMUSG00000025498	-1.322720054	3.90E-13	3.31E-09	3.428565104	3.96E-64	1.34E-60
Cxcl5	ENSMUSG00000029371	-1.199834605	6.50E-11	1.84E-07	3.370918298	3.3E-27	1.42E-24
Ccl7	ENSMUSG00000035373	-1.020396206	2.84E-06	0.001119	3.168049161	7.33E-18	8.62E-16
Isg15	ENSMUSG00000035692	-1.151876996	1.41E-08	1.83E-05	2.192186131	5.14E-22	9.46E-20
Saa3	ENSMUSG00000040026	-1.21478413	1.70E-08	1.92E-05	6.587536481	1.63E-80	1.38E-76
Saa1	ENSMUSG00000074115	-1.037241452	1.61E-06	0.000706582	4.344103762	5.13E-32	3.34E-29
Tgtp1	ENSMUSG00000078922	-1.126181149	7.50E-08	6.05E-05	1.653443678	9.49E-09	0.000000246
Gbp11	ENSMUSG00000092021	-1.160260065	9.11975E-08	6.71531E-05	2.140380325	1.16E-09	3.56E-08

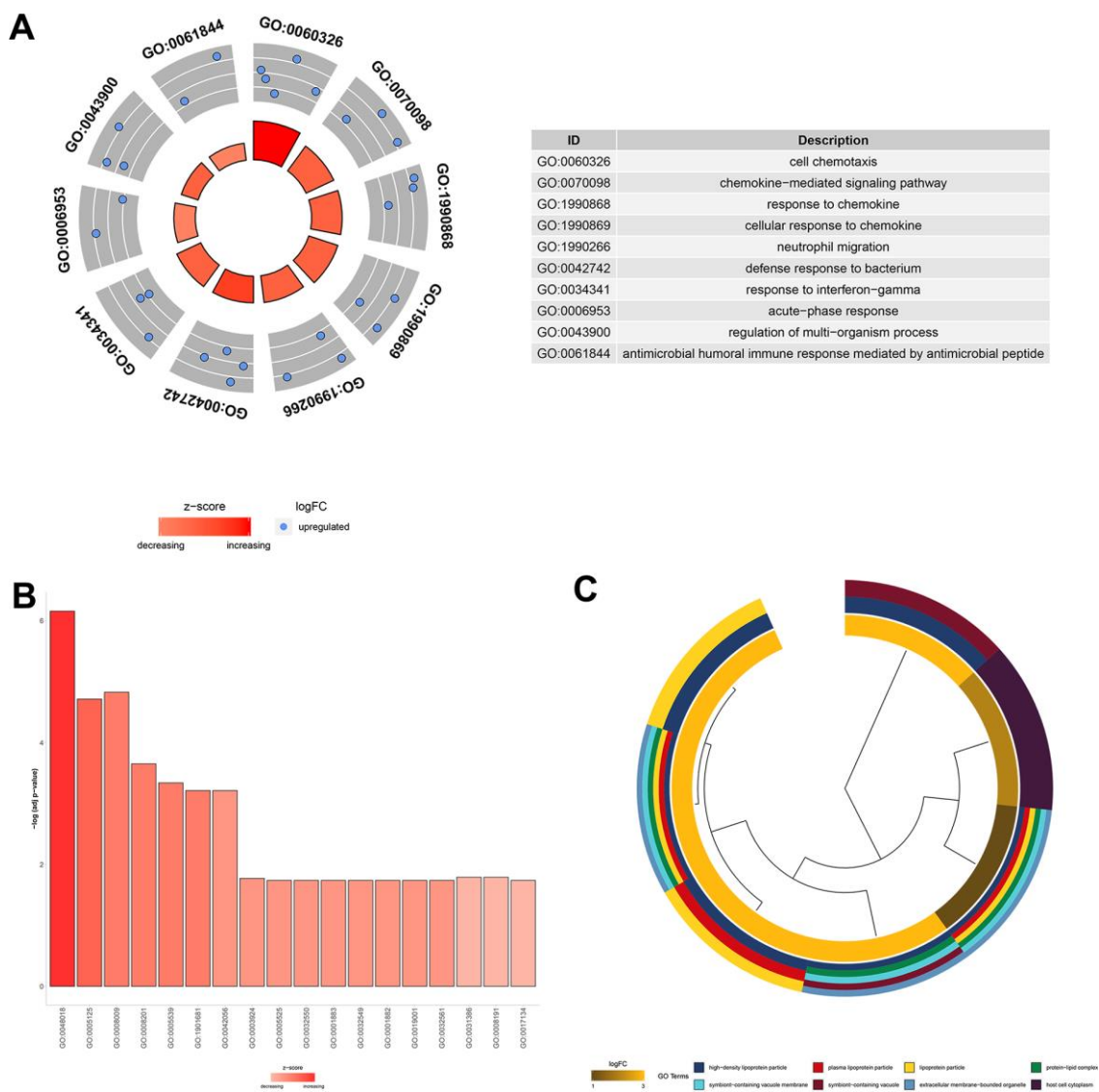| ID	Description
GO:0060326	cell chemotaxis
GO:0070098	chemokine−mediated signaling pathway
GO:1990868	response to chemokine
GO:1990869	cellular response to chemokine
GO:1990266	neutrophil migration
GO:0042742	defense response to bacterium
GO:0034341	response to interferon−gamma
GO:0006953	acute−phase response
GO:0043900	regulation of multi−organism process
GO:0061844	antimicrobial humoral immune response mediated by antimicrobial peptide

Figure 4. GO functional analysis of the 11 core DEGs related to the therapeutic effect of AST. (**A**) Top 10 significantly (P<0.05) enriched terms in biological processes. (**B**) Significantly (P<0.05) enriched terms in molecular functions. (**C**) Top 8 significantly (P<0.05) enriched terms in cellular components.
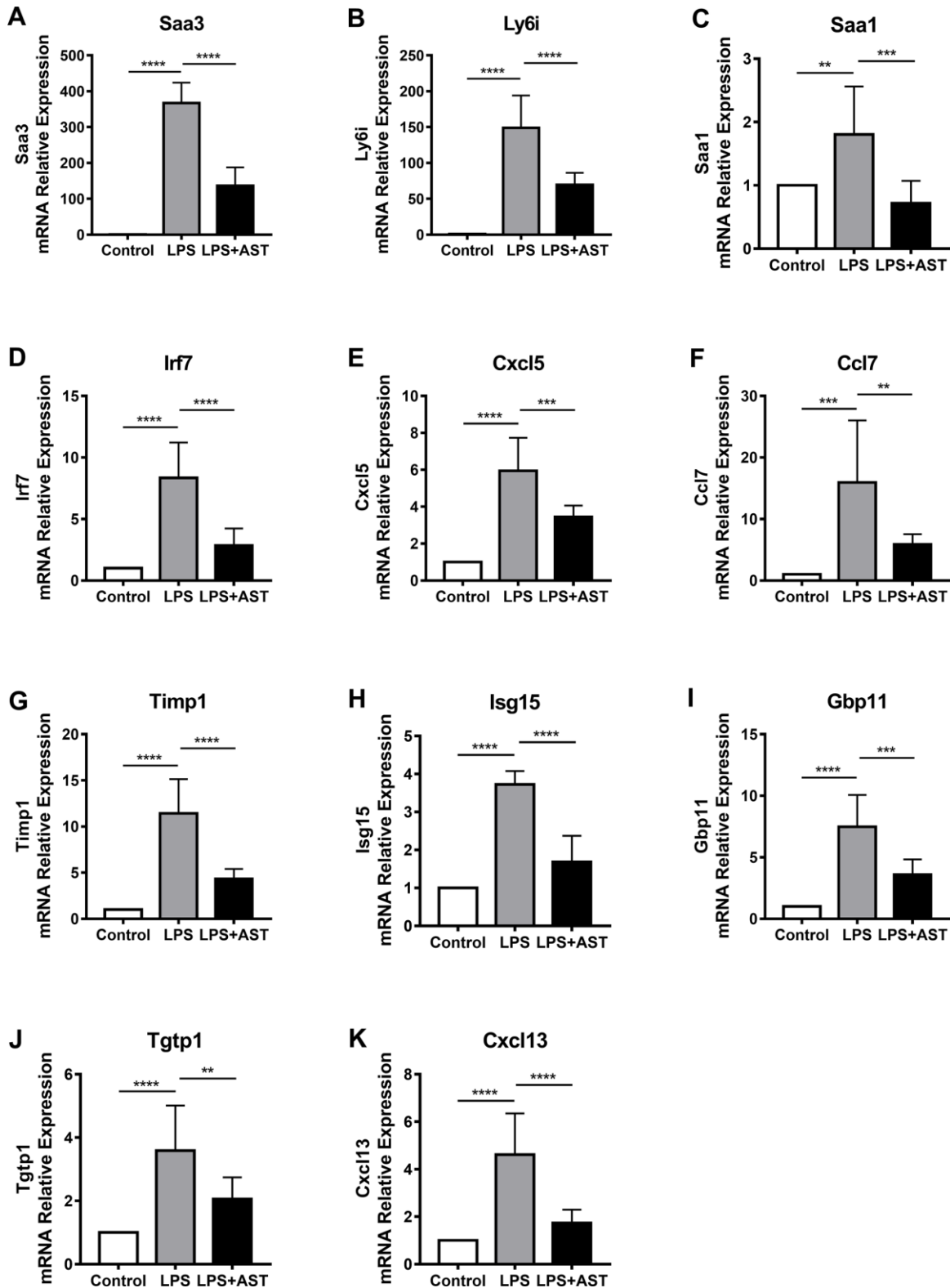
Figure 5. Changes in the expression of 11 core genes (A-K: *Saa3, Ly6i, Saa1, Irf7, Cxcl5, Ccl7, Timp1, Isg15, Gbp11, Tgtp1,* **and** *Cxcl13*) **in the lungs of an established mouse model.** Quantitative real-time polymerase chain reaction (RT-qPCR) was conducted to quantify the relative expression of the 11 core genes in the control group (n = 4), LPS-induced ALI group (n = 4), and AST treatment group (n = 4). GAPDH was used as an internal control gene. The experiments were performed at least in triplicate. The error bars represent the SEM. Statistical analysis of significant differences between groups was achieved with one-way ANOVA using Prism 7 software. ****p < 0.0001, ***p < 0.001, **p < 0.01, and *p < 0.05 were considered statistically significant.

induced by severe sepsis [32]. To reduce the study bias and increase the statistical power of individual microarray data, we performed a meta-analysis of five microarray gene expression profiles to assess the differentially expressed genes between LPS-induced and control groups. Consequently, 2097 differentially expressed genes (DEGs) were identified using three meta-analysis approaches. To further identify the robust expression signature related to LPS-induced ALI and investigate the transcriptional changes in response to the treatment of ALI by AST, we performed RNA-seq on three groups of mice and integrated the data with the results of the above mentioned meta-analysis. Ultimately, we identified 11 core DEGs that were significantly associated with AST treatment. *Saa3, Ly6i, Saa1, Irf7, Cxcl5, Ccl7, Timp1, Isg15, Gbp11, Tgtp1,* and *Cxcl13* were found to be overexpressed in the LPS group compared with the control group but relatively downregulated in the AST group. Our qRT-PCR and IHC verification of the 11 core genes in the mice suggested that these genes might be the key mediators of the therapeutic effect of AST in ALI/ARDS.

Among the 11 core genes that were differentially expressed in response to AST mediation, two genes are members of the serum amyloid A (SAA) family. SAA is a critical acute-phase protein that is often increased by infection, trauma, cancer, or other causes of inflammation and plays an important role in the regulation of inflammatory responses [33]. Recent studies have indicated that an increased level of SAA is positively correlated with the disease progression of COVID19, and can thus be a sensitive indicator for assessing the severity and prognosis of COVID-19 [34]. In our study, *Saa3* was the most significantly inhibited gene by AST application in LPS-induced ALI mice, and its downregulation was further confirmed by qRT-PCR and IHC. SAA3, the one of three isoforms of SAA expressed in mice, is stimulated intensely in LPS-induced acute systemic inflammation, which is consistent with our findings [35]. High expression of SAA3 in response to acute inflammation may be repressed by an interaction with noncoding RNAs. It has been confirmed that miR-30b-3p may target *Saa3* to protect against LPS-induced ALI [36]. Additionally, lncRNA MALAT1 can also target *Saa3* directly or indirectly to cause many diseases such as inflammation, diabetes and septic cardiomyocytes [37, 38]. SAA1, another member of the SAA gene family, is believed to have a pro-inflammatory effect, and its expression may aggravate tissue inflammation and damage [39]. Removing the N- and C-terminal sequences of SAA1 can switch the protein to an anti-inflammatory role [40]. However, other research has suggested that mice induced to express genetically modified human SAA1 have a partial protective effect against the inflammatory response and lung injury caused by LPS

[41]. Moreover, *Saa1* is the direct target of miR-660, which can protect nucleus pulposus cells from TNFa-induced apoptosis in intervertebral disc degeneration [42]. Considering that SAA might act as a biomarker of inflammatory disease, it is possible, that its down-regulation induced by AST may partly indicate the anti-inflammatory effect of AST. The deeper molecular mechanism underlying SAA action in response to AST application deserves further exploration.

Interferon regulatory factor 7 (IRF7) is considered the master regulator of IFN-α against pathogenic infections [43]. The excessive activation of IRF7 promotes the development of acute lung injury (ALI) caused by influenza A virus (IAV), and attenuating IRF7 activity can significantly prevent the progression of IAV-induced ALI in model mice [44]. Thus, the present finding that IRF7 was upregulated by LPS and downregulated in response to AST treatment may suggest that of AST protects against ALI.

Regarding how IRF7 regulates IFN production, miRNA may act as an important mediator. Previous research has shown that miR-302c can downregulate IRF3 and IRF7 expression to mediate influenza A virus-induced IFNβ expression [45]. Additionally, miR-144 was shown to reduces the antiviral response by attenuating the TRAF6-IRF7 pathway to alter the cellular antiviral transcriptional landscape [46]. However, whether miRNA-IRF7 interactions are involved in the pharmacological mechanism of AST remains to be further investigated.

Tissue inhibitor of metalloproteinase-1 (TIMP1), a member of TIMP family, is primarily recognized to regulate the degradation of the extracellular matrix by inhibiting the activity of matrix metalloproteinases (MMPs) [47]. It has been reported that an imbalance between MMP9 and TIMP1 plays a pivotal role in the pathogenesis of ARDS mainly through participating in airway remodeling, thus indicating the function of the MMP9/TIMP1 ratio in the evolution of pulmonary fibrosis in ARDS [48]. Indeed, increased systemic levels of TIMP1 were proven to be associated with increased 90-day mortality in ARDS patients according to a large, prospective, multicenter study [49]. Additionally, other research has demonstrated that increased TIMP1 expression promotes an immune response, has a pro-inflammatory effect in the lungs after influenza infection and facilitates an injurious phenotype [50]. The above observations not only support our present results regarding TIMP1 but also provide a considerable explanation for the increase in TIMP1 expression after LPS application. Intriguingly, given that TIMPs are highly expressed in liver fibrosis and that the imbalance of MMPs/TIMPs promotes the

progression of fibrosis, Shen et al. found that astaxanthin is able to repress the activation of hepatic stellate cells (HSCs) to ameliorate liver fibrosis through downregulating the expression of NF-κB and TGF-β1 and preserving the balance between MMP2 and TIMP1 [48]. Hence, it is reasonable to further investigate whether there is a similar mechanism by which AST downregulates the expression of TIMP1 to mitigate LPS-induced ALI.

Interferon-stimulated gene 15 (*Isg15*), which encodes the ubiquitin-like protein ISG15, which is primarily induced by type I interferons, is an essential player in regulating host signaling pathways such as damage repair responses and immune responses. ISG15 can be induced by various pathogenic stimuli such as viral and bacterial infections, lipopolysaccharide (LPS), retinoic acid, or certain genotoxic stressors [51]. In accordance with our findings, previous studies have observed increased levels of ISG15 conjugates in macrophages in response to LPS treatment [52]. Moreover, research has found that systemic *ISG* (*MX1, ISG15, IFIT1,* and *IFIT3*) expression within the first days of ARDS onset is associated with disease severity and prognosis. This response should be considered along with other identified genetic, environmental, and complex demographic factors as the cause of heterogeneity in ARDS prognosis [53]. Nevertheless, no data has been reported on the association between ISG15 and AST in the literature.

Since the excessive recruitment of leukocytes appears to be a central contributor to the pathogenesis of ALI, the elevation of proinflammatory cytokines and chemokines is considered the most important factor [54]. Similarly, we found that the expression of chemokines such as *Ccl7, Cxcl5,* and *Cxcl13* were increased after LPS instillation but decreased after AST treatment. Previous reports have documented an increased level of CCL7 in a mouse model of acute LPS-induced lung inflammation [55]. Moreover, the expression of CXCL5 is also rapidly induced in ALI murine models after LPS administration [56]. However, no data has on CXCL13 expression in ALI models has been reported. Therefore, we report for the first time the induction of CXCL13 after LPS administration, which provides insights into the role of CXCL13 in the pathogenesis of ALI. Furthermore, the observation of decreased expression of *Ccl7*, *Cxcl5*, and *Cxcl13* may hint at the anti-inflammatory properties of AST.

Although the roles of other DEGs (*Ly6i, Gbp11,* and *Tgtp1*) have been described in many other diseases in detail, their regulatory mechanisms in ALI-/ ARDS- are not fully understood. Our results show that these DEGs are overexpressed to varying degrees in the LPS group

and that AST can effectively prevent this over-expression. Further studies on the roles of these three genes in ALI initiation and progression are need. To determine the functional mechanisms of these 11 DEGs, GO enrichment analyses were further conducted. According to the results, 61 terms in biological process category, 18 in cellular component category and 15 in the molecular function category were enriched. The 5 most significantly enriched terms in the BP category were associated with chemokines and neutrophils, indicating the dominant role of neutrophils and related chemokines in the pathogenesis and progression of LPS-induced ALI. In ALI, the excessive recruitment of inflammatory cells and their mediators results in injury to endothelial and epithelial barriers [54]. Thus, agents such as AST, which can exert robust anti-inflammatory effects, may provide potential treatment prospects.

Despite this, several limitations of the current study need to be addressed. First, our research did not use the ALI mouse models induced by other agents; thus, it did not address heterogeneity of ALI initiation. Second, given that findings in animal models of LPS-induced lung injury may depend on the time point at which samples are obtained and physiological data are captured, the dynamic changes in LPS-induced ALI models may have been ignored to a certain extent [57]. Finally, in-depth research into the underlying mechanisms using knockout-gene mice for each differentially expressed gene will help further our understanding of the role of AST in ameliorating ALI/ARDS.

In conclusion, many genes were dysregulated in ALI/ARDS. We not only identified genes that consistently differed in expression in the LPS group compared to the control group but also revealed that AST can alleviate the abnormal expression of these genes and thus confer a certain therapeutic effect against ALI/ARDS, suggesting the potential for AST to become a novel treatment for ALI/ARDS.

MATERIALS AND METHODS

Microarray data meta-analysis

To identify the genes related to LPS-induced acute lung injury in mice, five datasets (GSE102016, GSE2 411, GSE16409, GSE104214, and GSE18341) were obtained from GEO (Gene Expression Omnibus, http://www.ncbi.nlm.nih.gov/geo) [58–62]. LPS and control treatments were used in this study. The detailed information (experimental design, transcriptome analysis, array information, data processing, and platform ID) for these datasets can be obtained from the GEO repository, and this information is partly

summarized in Table 1 and is described in more detail in Supplementary Table 1.

Then, we conducted a microarray meta-analysis using NetworkAnalyst 3.0 (https://www.networkanalyst.ca) [20]. NetworkAnalyst is a visual analytics platform for comprehensive gene expression profiling and meta-analysis. All gene probes were converted to a common Entrez ID using the gene/probe conversion tool in NetworkAnalyst. Following quantile normalization, all datasets were preprocessed through a log2 transformation and variance stabilizing normalization (VSN). Each dataset was visualized in box plots to ensure an identical distribution among the samples. Differential expression analysis was performed independently for each dataset using NetworkAnalyst, with an FDR of 0.05 and a significance of $p < 0.05$. The moderated t-test was based on the Limma algorithm. For the meta-analysis, we used Fisher's method, the fixed-effect model, and vote counting (combined $p < 0.05$ or vote counts ≥ 3 were considered significant) to identify the differentially expressed genes (DEGs) and we selected the common DEGs identified by these three methods as the final DEGs.

Animal materials

Male C57BL/6J mice (18–24g, 6~8-weeks-old) were purchased from Beijing Vital River Laboratory Animal Technology Co., Ltd. (Beijing, China). The mice were housed 5 per cage under a 12h light/dark cycle in a laboratory at 23 ± 2 °C and 50% humidity. All experiment protocols conformed to the guidelines of the China Council on Animal Care and Use. These animal studies were approved by the Institutional Animal Research Committee of Union Hospital.

The mice were randomly allocated into three groups: (1) the control group (n=10), which was exposed to PBS alone and received an intraperitoneal injection of sterile saline; (2) the LPS group (n=10), which was exposed to PBS containing 0.5 mg/mL LPS; and (3) the AST group (n=10), which was intraperitoneally injected with AST (10 mg/ml, dissolved in PBS) at a dosage of 50mg/kg body weight every day before one week of exposure to LPS to evaluate its preventive and protective effects [19, 63], and intraperitoneally injected with 100mg/kg AST (20 mg/ml, dissolved in PBS) 24 hours after LPS exposure in order to confirm the therapeutic effect of AST [16]. AST was obtained from Sigma-Aldrich (St Louis, MO, USA). For acute LPS exposure, mice were exposed to an aerosol of phosphate buffer saline (PBS) alone or PBS containing 0.5 mg/mL LPS for 2h, in a custom-built cuboidal chamber. The LPS solution was aerosolized with a constant output ultrasonic nebulizer (model: 402B, Yuwell, China) at a flow rate of 35ml/h.

LPS was purchased from Sigma–Aldrich (extracted from Escherichia coli O55: B5, L2880). The chamber was 20 cm long, 15 cm wide and 15 cm high.

RNA-seq library and sequencing

Total RNA was extracted from mouse lung tissue samples with TRIzol® Reagent (Invitrogen, CA) following the manufacturer's protocol. The concentration and purity of the RNA were measured by a Nanodrop2000 spectrophotometer (NanoDrop Technologies, Technologies, Wilmington, DE, USA), the RNA integrity was detected by agarose gel electrophoresis, and the RIN was determined using an Agilent2100 Bioanalyzer (Agilent Technologies, Santa Clara, CA, USA). The construction of a single library required a total of 5μg RNA with a concentration of ≥200ng/μL and an OD 260/280 ratio between

1.8 and 2.2. Then, oligo (dT) magnetic beads were subjected to capture mRNAs that contained poly-A tails from the total RNA. The resulting mRNAs were subsequently randomly broken into small fragments of approximately 200 bp by adding fragmentation buffer. The mRNA fragments functioned as the templates for double-stranded cDNA (dscDNA) synthesis using the SuperScript double-stranded cDNA synthesis kit (Invitrogen, CA, USA). Under the action of reverse transcriptase, a strand of cDNA was synthesized by using random primers with mRNA as a template, which was followed by two-strand synthesis to form a stable double-stranded structure. Since there was a cohesive terminus in the double-stranded cDNA structure, End Repair Mix was added to patch it into a blunt end, and an A base was added at the 3 'end to connect the y-shaped adaptor. To purify and enrich the dscDNA, 15 cycles of PCR were performed, and clean DNA beads were used to screen 200-300 bp bands. After quantification by TBS380 (Picogreen, Invitrogen, CA USA), high-throughput sequencing of the resulting libraries was performed on the Illumina HiSeq xten/NovaSeq 6000 sequencing platform (San Diego, CA, USA), and the sequencing read length was paired-end (PE) 150.

Quality control of raw data

To ensure the accuracy of the subsequent biological information analysis, the raw sequencing data generated from RNA-Seq was firstly filtered to obtain high-quality sequencing data (clean data) to ensure the smooth progress of the subsequent analysis. Quality control of the raw reads was performed using SeqPrep (https://github.com/jstjohn/SeqPrep) and Sickle (https://github.com/najoshi/sickle). The processes were as follows. The first step was to remove the adapter

from the reads and the reads that did not insert the fragment due to the self-connection of the adapter. Second, bases with a low quality (quality value less than 20) at the end of the sequence (3' end) were trimmed. If there was still a quality value of less than 10 for the remaining sequence, the whole sequence was discarded; otherwise, it was retained. Third, reads with N ratios over 10% and sequences with lengths less than 20 bp after quality trimming were also removed. Finally, the error rate (%), Q20 and Q30 values, GC-content (%), and sequence duplication levels of the generated clean reads were assessed [64].

Data process and DEG analysis

After filtering the raw data, the clean data were aligned to the mouse reference genome GRCm38 by 'Bowtie2' software [65]. Then, read summarization was calculated by the 'feature count' tool. Differently expressed genes (DEGs) between the LPS samples and control samples were identified by t-test using the 'DEseq2' R package, as were DEGs between the AST samples and LPS samples [66]. The raw P-value was adjusted to the false discovery rate by the Benjamini method, and a false discovery rate (FDR) $\leq$ 0.05 and |log2FC|$\geq$ 1 was chosen as the threshold.

Functional enrichment analyses of DEGs

Based on the hypergeometric distribution algorithm, GO (Gene Ontology, http://www.geneontology.org/) biological process (BP), molecular function (MF) and cell component (CC) pathway enrichment analyses were performed using the 'clusterprofler' R package [21]. A P-value $\leq$ 0.05 was set as the cutoff criterion.

RNA isolation and qRT-PCR validation

To validate the combined findings from RNA-seq and microarray meta-analysis, the expression of 11 core DEGs in the three groups was confirmed. RNAiso Plus reagent (Takara, Tokyo, Japan) was employed to extract total RNA from mouse lung tissues from each group, and reverse transcription was performed to obtain cDNA using PrimeScript™RT Master Mix (Takara, Tokyo, Japan) along with the gDNA Eraser kit (Takara, Tokyo, Japan). Relative mRNA expression levels were determined using RT-PCR performed on Bio-Rad CFX Maestro (Bio-Rad, USA) with TB Green® Premix Ex Taq™ II (Takara, Tokyo, Japan). All the above experimental steps were performed according to the manufacturer's instructions for the corresponding kit. Glyceraldehyde-3-phosphate dehydrogenase (GAPDH) was selected as the reference, and the primer sequences are presented in Supplementary Table 6. qRT-PCR was performed under the following conditions: 95 °C for 3

min, followed by 40 cycles at 95 °C for 30 s, 56 °C for 30 s, and 72 °C for 30 s. Each analysis was implemented in triplicate, and the relative expression levels of the target genes were calculated by employing the 2-ΔΔCt method [67].

Statistical analysis

INMEX and NetworkAnalyst were applied for the network-based microarray meta-analysis. For qPCR data, statistical analysis of differences between groups was achieved by one-way ANOVA using Prism 7 software (GraphPad Software Inc., San Diego, CA, USA). A two-tailed test was used for all data, and differences with a P-value <0.05 were considered significant.

Abbreviations

ARDS: acute respiratory distress syndrome; ALI: acute lung injury; LPS: lipopolysaccharide; ROS: reactive oxygen species; TXNIP: thioredoxin interacting protein; Trx: thioredoxin; NLRP3: nucleotide-binding domain-like receptor protein 3; IL-1β: interleukin-1β; TNF-α: tumor necrosis factor-α; iNOS: inducible nitric oxide synthase; COX2: cyclooxygenase-2; AST: astaxanthin; NF-κB: nuclear factor kappaB; NO: nitric oxide; PGE2: prostaglandin E2; NOS: nitric oxide synthase; Drp1: dynamin-related protein-1; GEO: gene expression omnibus; VSN: variance stabilizing normalization; FDR: false discovery rate; DEGs: differentially expressed genes; dscDNA: double-stranded cDNA; PCR: polymerase chain reaction; PE: paired-end; GO: gene ontology; BP: biological process; MF: molecular function; CC: cell component; RT-PCR: reverse transcription-polymerase chain reaction; GAPDH: glyceraldehyde-3-phosphate dehydrogenase; qRT-PCR: quantitative real-time polymerase chain reaction; IHC: immunohistochemistry; ANOVA: analysis of variance; RNA-seq: RNA-sequencing; IPF: idiopathic pulmonary fibrosis; ZBP1: Z-DNA binding protein 1; SAA: serum amyloid A; COVID19: corona virus disease 19; MALAT1: metastasis associated lung adenocarcinoma transcript 1; IRF7: interferon regulatory factor 7; IAV: influenza A virus; TRAF6: TNF receptor associated factor 6; TIMP1: tissue inhibitor of metalloproteinase-1; MMPs: matrix metalloproteinases; HSCs: hepatic stellate cells; ISG15: interferon-stimulated gene 15; IFIT: interferon induced protein with tetratricopeptide repeats.

AUTHOR CONTRIBUTIONS

Kaimin Mao, Wei Geng and Yuhan Liao performed the animal experiments and conduct data analysis; Ping Luo and Pei Ma participated in the animal experiments. Hua Zhong, Juanjuan Xu and Shuai Zhang contributed to the data analysis. Yang Jin designed the experiments.

Kaimin Mao, Wei Geng and Yuhan Liao wrote the manuscript. Qi Tan1 and Qi Huang provided comments during the writing. Yang Jin revised the manuscript. All authors reviewed and approved the final manuscript.

CONFLICTS OF INTEREST

The authors declare that they have no conflicts interest.

FUNDING

REFERENCES

1. Thompson BT, Chambers RC, Liu KD. Acute respiratory distress syndrome. N Engl J Med. 2017; 377:562–72.
https://doi.org/10.1056/NEJMra1608077
PMID:28792873

2. Ashbaugh DG, Bigelow DB, Petty TL, Levine BE. Ashbaugh DG, bigelow DB, petty TL, levine BE. Acute respiratory distress in adults. The lancet, saturday 12 august 1967. Crit Care Resusc. 2005; 7:60–61.
PMID:16548822

3. Ware LB, Matthay MA. The acute respiratory distress syndrome. N Engl J Med. 2000; 342:1334–49.
https://doi.org/10.1056/NEJM200005043421806
PMID:10793167

4. Raetz CR, Whitfield C. Lipopolysaccharide endotoxins. Annu Rev Biochem. 2002; 71:635–700.
https://doi.org/10.1146/annurev.biochem.71.110601.135414 PMID:12045108

5. Lei J, Wei Y, Song P, Li Y, Zhang T, Feng Q, Xu G. Cordycepin inhibits LPS-induced acute lung injury by inhibiting inflammation and oxidative stress. Eur J Pharmacol. 2018; 818:110–14.
https://doi.org/10.1016/j.ejphar.2017.10.029
PMID:29054740

6. Lv H, Liu Q, Wen Z, Feng H, Deng X, Ci X. Xanthohumol ameliorates lipopolysaccharide (LPS)-induced acute lung injury via induction of AMPK/GSK3β-Nrf2 signal axis. Redox Biol. 2017; 12:311–24.
https://doi.org/10.1016/j.redox.2017.03.001
PMID:28285192

7. Han X, Wu YC, Meng M, Sun QS, Gao SM, Sun H. Linarin prevents LPS-induced acute lung injury by suppressing oxidative stress and inflammation via inhibition of TXNIP/NLRP3 and NF-κB pathways. Int J Mol Med. 2018; 42:1460–72.
https://doi.org/10.3892/ijmm.2018.3710
PMID:29845284

8. Ding XQ, Wu WY, Jiao RQ, Gu TT, Xu Q, Pan Y, Kong LD. Curcumin and allopurinol ameliorate fructose-induced hepatic inflammation in rats via miR-200a-mediated TXNIP/NLRP3 inflammasome inhibition. Pharmacol Res. 2018; 137:64–75.
https://doi.org/10.1016/j.phrs.2018.09.021
PMID:30248460

9. Shan Q, Zheng GH, Han XR, Wen X, Wang S, Li MQ, Zhuang J, Zhang ZF, Hu B, Zhang Y, Zheng YL. Troxerutin protects kidney tissue against BDE-47-induced inflammatory damage through CXCR4-TXNIP/NLRP3 signaling. Oxid Med Cell Longev. 2018; 2018:9865495.
https://doi.org/10.1155/2018/9865495
PMID:29849929

10. Liu Y, Lou G, Li A, Zhang T, Qi J, Ye D, Zheng M, Chen Z. AMSC-derived exosomes alleviate lipopolysaccharide/d-galactosamine-induced acute liver failure by miR-17-mediated reduction of TXNIP/NLRP3 inflammasome activation in macrophages. EBioMedicine. 2018; 36:140–50.
https://doi.org/10.1016/j.ebiom.2018.08.054
PMID:30197023

11. Zhong WJ, Yang HH, Guan XX, Xiong JB, Sun CC, Zhang CY, Luo XQ, Zhang YF, Zhang J, Duan JX, Zhou Y, Guan CX. Inhibition of glycolysis alleviates lipopolysaccharide-induced acute lung injury in a mouse model. J Cell Physiol. 2019; 234:4641–54.
https://doi.org/10.1002/jcp.27261
PMID:30256406

12. Higuera-Ciapara I, Félix-Valenzuela L, Goycoolea FM. Astaxanthin: a review of its chemistry and applications. Crit Rev Food Sci Nutr. 2006; 46:185–96.
https://doi.org/10.1080/10408690590957188
PMID:16431409

13. Hussein G, Sankawa U, Goto H, Matsumoto K, Watanabe H. Astaxanthin, a carotenoid with potential in human health and nutrition. J Nat Prod. 2006; 69:443–49.
https://doi.org/10.1021/np050354+ PMID:16562856

14. Routray W, Dave D, Cheema SK, Ramakrishnan VV, Pohling J. Biorefinery approach and environment-friendly extraction for sustainable production of astaxanthin from marine wastes. Crit Rev Biotechnol. 2019; 39:469–88.
https://doi.org/10.1080/07388551.2019.1573798

PMID:30939937

15. Lee SJ, Bai SK, Lee KS, Namkoong S, Na HJ, Ha KS, Han JA, Yim SV, Chang K, Kwon YG, Lee SK, Kim YM. Astaxanthin inhibits nitric oxide production and inflammatory gene expression by suppressing I(kappa)B kinase-dependent NF-kappaB activation. Mol Cells. 2003; 16:97–105.
PMID:14503852

16. Ohgami K, Shiratori K, Kotake S, Nishida T, Mizuki N, Yazawa K, Ohno S. Effects of astaxanthin on lipopolysaccharide-induced inflammation in vitro and in vivo. Invest Ophthalmol Vis Sci. 2003; 44:2694–701.
https://doi.org/10.1167/iovs.02-0822
PMID:12766075

17. Zhang J, Xu P, Wang Y, Wang M, Li H, Lin S, Mao C, Wang B, Song X, Lv C. Astaxanthin prevents pulmonary fibrosis by promoting myofibroblast apoptosis dependent on Drp1-mediated mitochondrial fission. J Cell Mol Med. 2015; 19:2215–31.
https://doi.org/10.1111/jcmm.12609 PMID:26119034

18. Bi J, Cui R, Li Z, Liu C, Zhang J. Astaxanthin alleviated acute lung injury by inhibiting oxidative/nitrative stress and the inflammatory response in mice. Biomed Pharmacother. 2017; 95:974–82.
https://doi.org/10.1016/j.biopha.2017.09.012
PMID:28915539

19. Cai X, Chen Y, Xie X, Yao D, Ding C, Chen M. Astaxanthin prevents against lipopolysaccharide-induced acute lung injury and sepsis via inhibiting activation of MAPK/NF-κB. Am J Transl Res. 2019; 11:1884–94.
PMID:30972212

20. Zhou G, Soufan O, Ewald J, Hancock RE, Basu N, Xia J. NetworkAnalyst 3.0: a visual analytics platform for comprehensive gene expression profiling and meta-analysis. Nucleic Acids Res. 2019; 47:W234–41.
https://doi.org/10.1093/nar/gkz240
PMID:30931480

21. Yu G, Wang LG, Han Y, He QY. clusterProfiler: an R package for comparing biological themes among gene clusters. OMICS. 2012; 16:284–87.
https://doi.org/10.1089/omi.2011.0118
PMID:22455463

22. Goodman RB, Strieter RM, Martin DP, Steinberg KP, Milberg JA, Maunder RJ, Kunkel SL, Walz A, Hudson LD, Martin TR. Inflammatory cytokines in patients with persistence of the acute respiratory distress syndrome. Am J Respir Crit Care Med. 1996; 154:602–11.
https://doi.org/10.1164/ajrccm.154.3.8810593
PMID:8810593

23. Potey PM, Rossi AG, Lucas CD, Dorward DA. Neutrophils in the initiation and resolution of acute pulmonary inflammation: understanding biological function and therapeutic potential. J Pathol. 2019; 247:672–85.
https://doi.org/10.1002/path.5221 PMID:30570146

24. Williams AE, José RJ, Mercer PF, Brealey D, Parekh D, Thickett DR, O'Kane C, McAuley DF, Chambers RC. Evidence for chemokine synergy during neutrophil migration in ARDS. Thorax. 2017; 72:66–73.
https://doi.org/10.1136/thoraxjnl-2016-208597
PMID:27496101

25. Cripps JG, Crespo FA, Romanovskis P, Spatola AF, Fernández-Botrán R. Modulation of acute inflammation by targeting glycosaminoglycan-cytokine interactions. Int Immunopharmacol. 2005; 5:1622–32.
https://doi.org/10.1016/j.intimp.2005.04.010
PMID:16039552

26. Grommes J, Soehnlein O. Contribution of neutrophils to acute lung injury. Mol Med. 2011; 17:293–307.
https://doi.org/10.2119/molmed.2010.00138
PMID:21046059

27. Cabrera-Benitez NE, Pérez-Roth E, Casula M, Ramos-Nuez A, Ríos-Luci C, Rodríguez-Gallego C, Sologuren I, Jakubkiene V, Slutsky AS, Padrón JM, Villar J. Anti-inflammatory activity of a novel family of aryl ureas compounds in an endotoxin-induced airway epithelial cell injury model. PLoS One. 2012; 7:e48468.
https://doi.org/10.1371/journal.pone.0048468
PMID:23144889

28. Vuga LJ, Tedrow JR, Pandit KV, Tan J, Kass DJ, Xue J, Chandra D, Leader JK, Gibson KF, Kaminski N, Sciurba FC, Duncan SR. C-X-C motif chemokine 13 (CXCL13) is a prognostic biomarker of idiopathic pulmonary fibrosis. Am J Respir Crit Care Med. 2014; 189:966–74.
https://doi.org/10.1164/rccm.201309-1592OC
PMID:24628285

29. Kuriakose T, Kanneganti TD. ZBP1: innate sensor regulating cell death and inflammation. Trends Immunol. 2018; 39:123–34.
https://doi.org/10.1016/j.it.2017.11.002
PMID:29236673

30. Bao Y, Gao Y, Shi Y, Cui X. Dynamic gene expression analysis in a H1N1 influenza virus mouse pneumonia model. Virus Genes. 2017; 53:357–66.
https://doi.org/10.1007/s11262-017-1438-y
PMID:28243843

31. Liu X, Das AM, Seideman J, Griswold D, Afuh CN, Kobayashi T, Abe S, Fang Q, Hashimoto M, Kim H, Wang X, Shen L, Kawasaki S, Rennard SI. The CC chemokine ligand 2 (CCL2) mediates fibroblast survival through IL-6. Am J Respir Cell Mol Biol. 2007; 37:121–28.
https://doi.org/10.1165/rcmb.2005-0253OC

PMID:17379849

32. Silasi-Mansat R, Zhu H, Georgescu C, Popescu N, Keshari RS, Peer G, Lupu C, Taylor FB, Pereira HA, Kinasewitz G, Lambris JD, Lupu F. Complement inhibition decreases early fibrogenic events in the lung of septic baboons. J Cell Mol Med. 2015; 19:2549–63. https://doi.org/10.1111/jcmm.12667 PMID:26337158

33. De Buck M, Gouwy M, Wang JM, Van Snick J, Proost P, Struyf S, Van Damme J. The cytokine-serum amyloid a-chemokine network. Cytokine Growth Factor Rev. 2016; 30:55–69. https://doi.org/10.1016/j.cytogfr.2015.12.010 PMID:26794452

34. Li H, Xiang X, Ren H, Xu L, Zhao L, Chen X, Long H, Wang Q, Wu Q. Serum amyloid A is a biomarker of severe coronavirus disease and poor prognosis. J Infect. 2020; 80:646–55. https://doi.org/10.1016/j.jinf.2020.03.035 PMID:32277967

35. Tannock LR, De Beer MC, Ji A, Shridas P, Noffsinger VP, den Hartigh L, Chait A, De Beer FC, Webb NR. Serum amyloid A3 is a high density lipoprotein-associated acute-phase protein. J Lipid Res. 2018; 59:339–47. https://doi.org/10.1194/jlr.M080887 PMID:29247043

36. Yi X, Wei X, Lv H, An Y, Li L, Lu P, Yang Y, Zhang Q, Yi H, Chen G. Exosomes derived from microRNA-30b-3p-overexpressing mesenchymal stem cells protect against lipopolysaccharide-induced acute lung injury by inhibiting SAA3. Exp Cell Res. 2019; 383:111454. https://doi.org/10.1016/j.yexcr.2019.05.035 PMID:31170401

37. Puthanveetil P, Chen S, Feng B, Gautam A, Chakrabarti S. Long non-coding RNA MALAT1 regulates hyperglycaemia induced inflammatory process in the endothelial cells. J Cell Mol Med. 2015; 19:1418–25. https://doi.org/10.1111/jcmm.12576 PMID:25787249

38. Zhuang YT, Xu DY, Wang GY, Sun JL, Huang Y, Wang SZ. IL-6 induced lncRNA MALAT1 enhances TNF-α expression in LPS-induced septic cardiomyocytes via activation of SAA3. Eur Rev Med Pharmacol Sci. 2017; 21:302–09. PMID:28165557

39. Ye RD, Sun L. Emerging functions of serum amyloid a in inflammation. J Leukoc Biol. 2015; 98:923–29. https://doi.org/10.1189/jlb.3VMR0315-080R PMID:26130702

40. Zhou H, Chen M, Zhang G, Ye RD. Suppression of lipopolysaccharide-induced inflammatory response by fragments from serum amyloid a. J Immunol. 2017; 199:1105–12. https://doi.org/10.4049/jimmunol.1700470 PMID:28674180

41. Cheng N, Liang Y, Du X, Ye RD. Serum amyloid a promotes LPS clearance and suppresses LPS-induced inflammation and tissue injury. EMBO Rep. 2018; 19:e45517. https://doi.org/10.15252/embr.201745517 PMID:30126923

42. Zhang HJ, Ma XH, Xie SL, Qin SL, Liu CZ, Zhang ZG. Knockdown of miR-660 protects nucleus pulposus cells from TNF-a-induced apoptosis by targeting serum amyloid A1. J Orthop Surg Res. 2020; 15:7. https://doi.org/10.1186/s13018-019-1538-6 PMID:31907065

43. Ning S, Pagano JS, Barber GN. IRF7: activation, regulation, modification and function. Genes Immun. 2011; 12:399–414. https://doi.org/10.1038/gene.2011.21 PMID:21490621

44. Yang L, Tu L, Zhao P, Wang Y, Wang S, Lu W, Wang Y, Li X, Yu Y, Hua S, Wang L. Attenuation of interferon regulatory factor 7 activity in local infectious sites of trachea and lung for preventing the development of acute lung injury caused by influenza a virus. Immunology. 2019; 157:37–51. https://doi.org/10.1111/imm.13045 PMID:30667045

45. Gui S, Chen X, Zhang M, Zhao F, Wan Y, Wang L, Xu G, Zhou L, Yue X, Zhu Y, Liu S. Mir-302c mediates influenza a virus-induced IFNβ expression by targeting NF-κB inducing kinase. FEBS Lett. 2015; 589:4112–18. https://doi.org/10.1016/j.febslet.2015.11.011 PMID:26602079

46. Rosenberger CM, Podyminogin RL, Diercks AH, Treuting PM, Peschon JJ, Rodriguez D, Gundapuneni M, Weiss MJ, Aderem A. miR-144 attenuates the host response to influenza virus by targeting the TRAF6-IRF7 signaling axis. PLoS Pathog. 2017; 13:e1006305. https://doi.org/10.1371/journal.ppat.1006305 PMID:28380049

47. Ries C. Cytokine functions of TIMP-1. Cell Mol Life Sci. 2014; 71:659–72. https://doi.org/10.1007/s00018-013-1457-3 PMID:23982756

48. Lanchou J, Corbel M, Tanguy M, Germain N, Boichot E, Theret N, Clement B, Lagente V, Malledant Y. Imbalance between matrix metalloproteinases (MMP-9 and MMP-2) and tissue inhibitors of metalloproteinases (TIMP-1 and TIMP-2) in acute respiratory distress syndrome patients. Crit Care Med. 2003; 31:536–42. https://doi.org/10.1097/01.CCM.0000048626.02184.F8

PMID:12576963

49. Hästbacka J, Linko R, Tervahartiala T, Varpula T, Hovilehto S, Parviainen I, Vaara ST, Sorsa T, Pettilä V. Serum MMP-8 and TIMP-1 in critically ill patients with acute respiratory failure: TIMP-1 is associated with increased 90-day mortality. Anesth Analg. 2014; 118:790–98.
https://doi.org/10.1213/ANE.0000000000000120
PMID:24651234

50. Allen JR, Ge L, Huang Y, Brauer R, Parimon T, Cassel SL, Sutterwala FS, Chen P. TIMP-1 promotes the immune response in influenza-induced acute lung injury. Lung. 2018; 196:737–43.
https://doi.org/10.1007/s00408-018-0154-2
PMID:30167842

51. Perng YC, Lenschow DJ. ISG15 in antiviral immunity and beyond. Nat Rev Microbiol. 2018; 16:423–39.
https://doi.org/10.1038/s41579-018-0020-5
PMID:29769653

52. Malakhova O, Malakhov M, Hetherington C, Zhang DE. Lipopolysaccharide activates the expression of ISG15-specific protease UBP43 via interferon regulatory factor 3. J Biol Chem. 2002; 277:14703–11.
https://doi.org/10.1074/jbc.M111527200
PMID:11854279

53. Nick JA, Caceres SM, Kret JE, Poch KR, Strand M, Faino AV, Nichols DP, Saavedra MT, Taylor-Cousar JL, Geraci MW, Burnham EL, Fessler MB, Suratt BT, et al. Extremes of interferon-stimulated gene expression associate with worse outcomes in the acute respiratory distress syndrome. PLoS One. 2016; 11:e0162490.
https://doi.org/10.1371/journal.pone.0162490
PMID:27606687

54. Bhatia M, Zemans RL, Jeyaseelan S. Role of chemokines in the pathogenesis of acute lung injury. Am J Respir Cell Mol Biol. 2012; 46:566–72.
https://doi.org/10.1165/rcmb.2011-0392TR
PMID:22323365

55. Mercer PF, Williams AE, Scotton CJ, José RJ, Sulikowski M, Moffatt JD, Murray LA, Chambers RC. Proteinase-activated receptor-1, CCL2, and CCL7 regulate acute neutrophilic lung inflammation. Am J Respir Cell Mol Biol. 2014; 50:144–57.
https://doi.org/10.1165/rcmb.2013-0142OC
PMID:23972264

56. Shah D, Romero F, Stafstrom W, Duong M, Summer R. Extracellular ATP mediates the late phase of neutrophil recruitment to the lung in murine models of acute lung injury. Am J Physiol Lung Cell Mol Physiol. 2014; 306:L152–61.
https://doi.org/10.1152/ajplung.00229.2013

PMID:24285266

57. Domscheit H, Hegeman MA, Carvalho N, Spieth PM. Molecular dynamics of lipopolysaccharide-induced lung injury in rodents. Front Physiol. 2020; 11:36.
https://doi.org/10.3389/fphys.2020.00036
PMID:32116752

58. Altemeier WA, Matute-Bello G, Gharib SA, Glenny RW, Martin TR, Liles WC. Modulation of lipopolysaccharide-induced gene transcription and promotion of lung injury by mechanical ventilation. J Immunol. 2005; 175:3369–76.
https://doi.org/10.4049/jimmunol.175.5.3369
PMID:16116230

59. Britto CJ, Niu N, Khanal S, Huleihel L, Herazo-Maya JD, Thompson A, Sauler M, Slade MD, Sharma L, Dela Cruz CS, Kaminski N, Cohn LE. BPIFA1 regulates lung neutrophil recruitment and interferon signaling during acute inflammation. Am J Physiol Lung Cell Mol Physiol. 2019; 316:L321–33.
https://doi.org/10.1152/ajplung.00056.2018
PMID:30461288

60. Shi Q, Fijten RR, Spina D, Riffo Vasquez Y, Arlt VM, Godschalk RW, Van Schooten FJ. Altered gene expression profiles in the lungs of benzo[a]pyrene-exposed mice in the presence of lipopolysaccharide-induced pulmonary inflammation. Toxicol Appl Pharmacol. 2017; 336:8–19.
https://doi.org/10.1016/j.taap.2017.09.023
PMID:28987381

61. Smith LS, Gharib SA, Frevert CW, Martin TR. Effects of age on the synergistic interactions between lipopolysaccharide and mechanical ventilation in mice. Am J Respir Cell Mol Biol. 2010; 43:475–86.
https://doi.org/10.1165/rcmb.2009-0039OC
PMID:19901347

62. Snyder JC, Reynolds SD, Hollingsworth JW, Li Z, Kaminski N, Stripp BR. Clara cells attenuate the inflammatory response through regulation of macrophage behavior. Am J Respir Cell Mol Biol. 2010; 42:161–71.
https://doi.org/10.1165/rcmb.2008-0353OC
PMID:19423773

63. Kubo H, Asai K, Kojima K, Sugitani A, Kyomoto Y, Okamoto A, Yamada K, Ijiri N, Watanabe T, Hirata K, Kawaguchi T. Astaxanthin suppresses cigarette smoke-induced emphysema through Nrf2 activation in mice. Mar Drugs. 2019; 17:673.
https://doi.org/10.3390/md17120673
PMID:31795292

64. Chen S, Zhou Y, Chen Y, Gu J. Fastp: an ultra-fast all-in-one FASTQ preprocessor. Bioinformatics. 2018; 34:i884–90.

https://doi.org/10.1093/bioinformatics/bty560
PMID:30423086

65. Langmead B, Salzberg SL. Fast gapped-read alignment with bowtie 2. Nat Methods. 2012; 9:357–59.
https://doi.org/10.1038/nmeth.1923
PMID:22388286

66. Love MI, Huber W, Anders S. Moderated estimation of fold change and dispersion for RNA-seq data with DESeq2. Genome Biol. 2014; 15:550.
https://doi.org/10.1186/s13059-014-0550-8
PMID:25516281

67. Livak KJ, Schmittgen TD. Analysis of relative gene expression data using real-time quantitative PCR and the 2(-Delta Delta C(T)) method. Methods. 2001; 25:402–08.
https://doi.org/10.1006/meth.2001.1262
PMID:11846609

SUPPLEMENTARY MATERIALS

Supplementary Materials and Methods

Microarray data meta-analysis

First of all, we used the search formula of LPS[All Fields] AND ("lung"[MeSH Terms] OR lung[All Fields]) AND ("Mus musculus"[Organism] AND "Expression profiling by array"[Filter]) to obtain 62 results in GEO DataSets. By eliminating datasets of miRNA sequencings, datasets not related to acute lung injury, and datasets that only researching on RNA sequencing of specific cells such as macrophages and type II alveolar epithelial cells, there were 8 articles remained (GSE71648, GSE104214, GSE102016, GSE38014, GSE18341, GSE16409, GSE11662 and GSE2411). Continuing to check the specific description of the sample in articles, we found some datasets were grouped with sample of n<3 and some mainly studied ALI or ARDS induced by excessive ventilation or non-LPS chemicals. In the end, there were 5 datasets (GSE102016, GSE2411, GSE16409, GSE104214 and GSE18341) that met the requirements of integrated analysis.

We conducted a microarray meta-analysis using NetworkAnalyst 3.0 combined three well-established meta-analysis approaches --Fisher's method, Fixed effect model, and Vote counting. The features and main characteristics are given below (https://www.networkanalyst.ca). (1) Fisher's method $(-2*\sum Log(p))$ is known as a 'weight-free' method and combines p values from multiple studies for information integration. (2) Effect size is the difference between two group means divided by standard deviation, which are considered combinable and comparable across different studies. In the fixed effects models (FEM), the estimated effect size in each study is assumed to come from an underlying true effect size plus measurement error. (3) Vote counting is the simplest method in meta-analysis. Differentially expressed gene is first selected based on a threshold to obtain a list of DE genes for each study. The vote for each gene can then be calculated as the total number of times it occurred in all DE lists. The final DE genes can be selected based on the minimal number of votes set by the user.

Immunohistochemistry

After the mice were sacrificed, the lung tissues were collected. Immediately, the tissue was fixed in 4% paraformaldehyde for 24 hours and embedded in paraffin. The embedded tissue was sliced into 5 µm sections for staining. After the tissue sections were deparaffinized and rehydrated, they were heated in citrate buffer at 121 °C for 30 minutes to restore antigen activity. The sections were then incubated with 0.3% hydrogen peroxide in methanol for 30 minutes to inhibit endogenous peroxidase activity. After blocking nonspecific reactions with 10% normal bovine serum, the sections were incubated with rabbit polyclonal antibodies specific for Ccl7 (1:100, Abcam), Saa3 (1:50, ab231680, Abcam), Ly6i (1:2000, Abcam), Saa1 (1:100-1:200, Thermo), lrf7 (1:100, Thermo), Timp1 (1:100, Thermo), Isg15 (1:100, Thermo) and Cxcl13 (1:1000, Abcam). The treated samples were placed at 4 °C for 12 hours. The sections were then washed with PBS and incubated with horseradish peroxidase-conjugated secondary antibodies at 37 °C for 2 hours. The stained sections were imaged under an inverted phase contrast microscope.
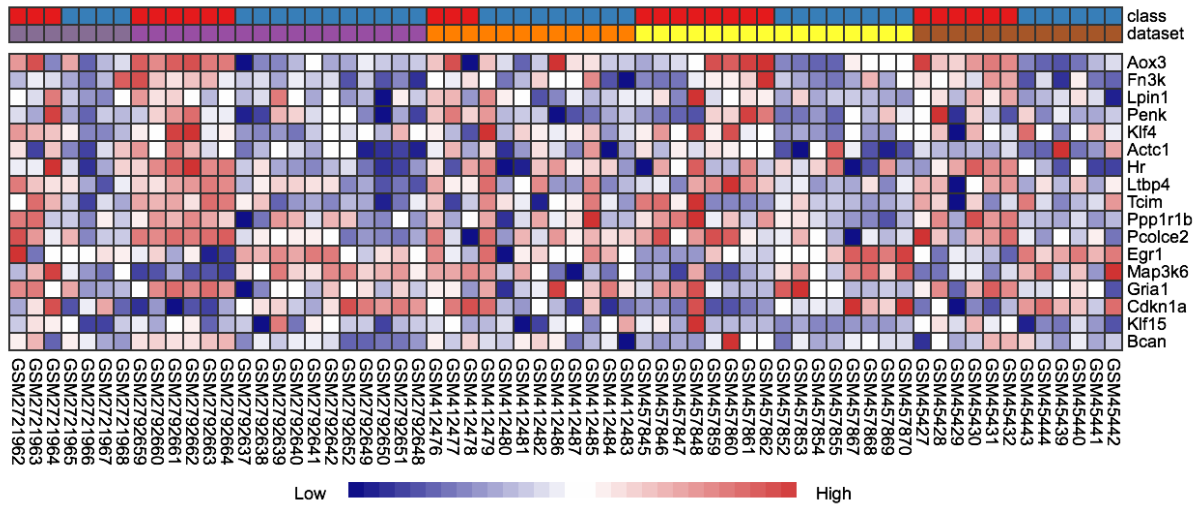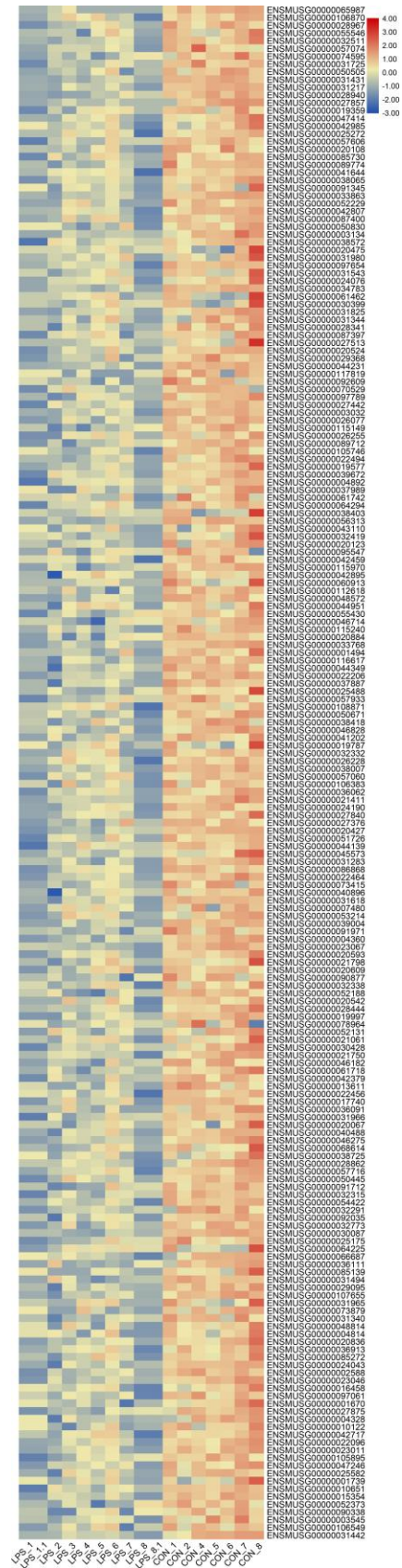
Supplementary Figure 1. Heat map of the 17 overlapping downregulated genes identified by both meta-analysis of published microarrays and our RNA sequencing experiments (control group vs. LPS group).
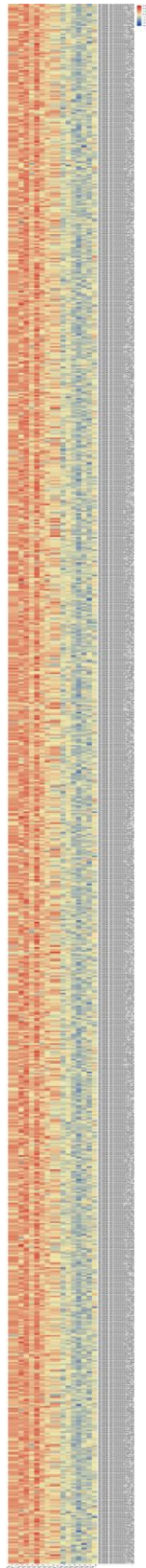
Supplementray Figure 2-1. Heat map of the 989 significantly upregulated genes in the LPS group compared to the control group identified by RNA sequencing.

Supplementary Figure 2-2. Heat map of the 198 significantly downregulated genes in the LPS group compared to the control group identified by RNA sequencing.
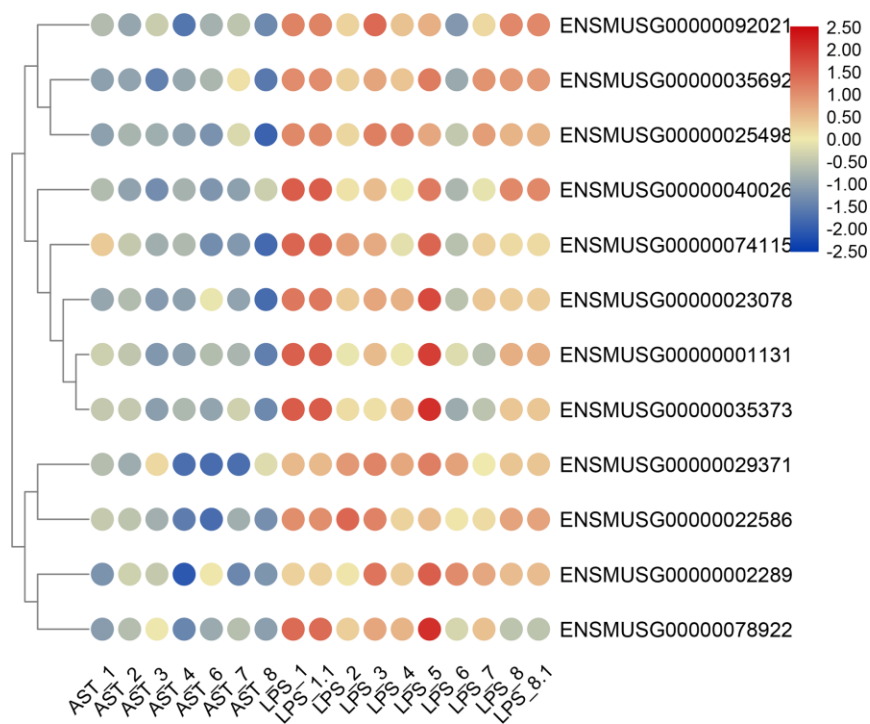
Supplementary Figure 3-1. Heat map of the 9 significantly upregulated genes in the AST group compared to the LPS group identified by RNA sequencing.
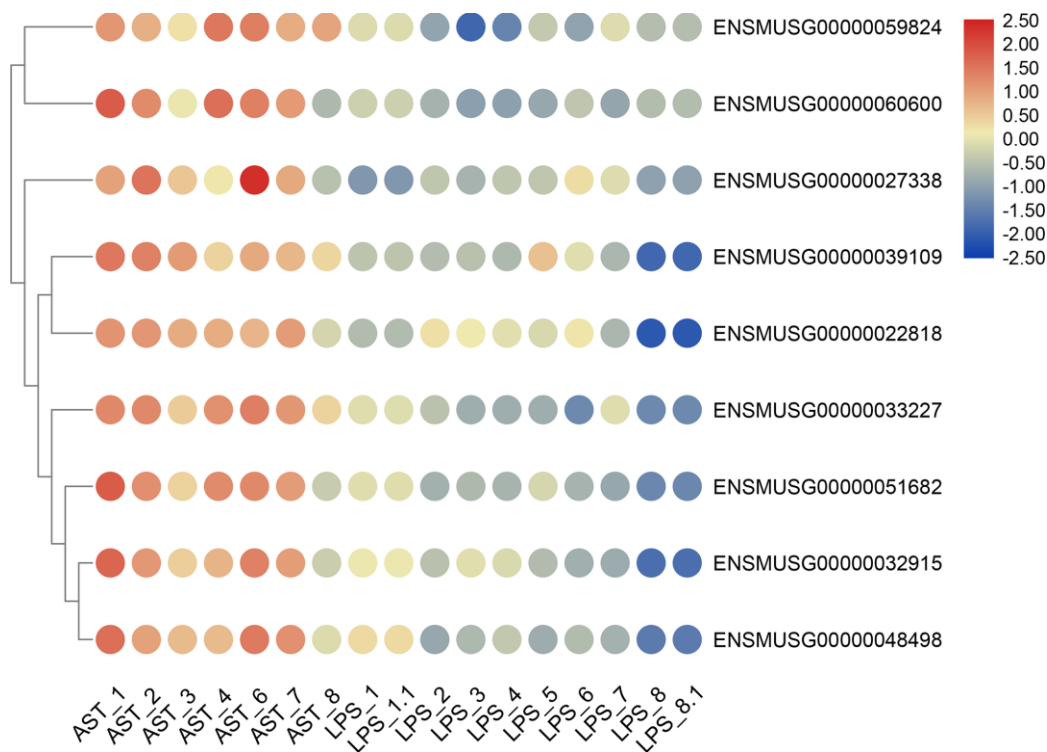

Supplementary Figure 3-2. Heat map of the 12 significantly downregulated genes in the AST group compared to the LPS group identified RNA sequencing.
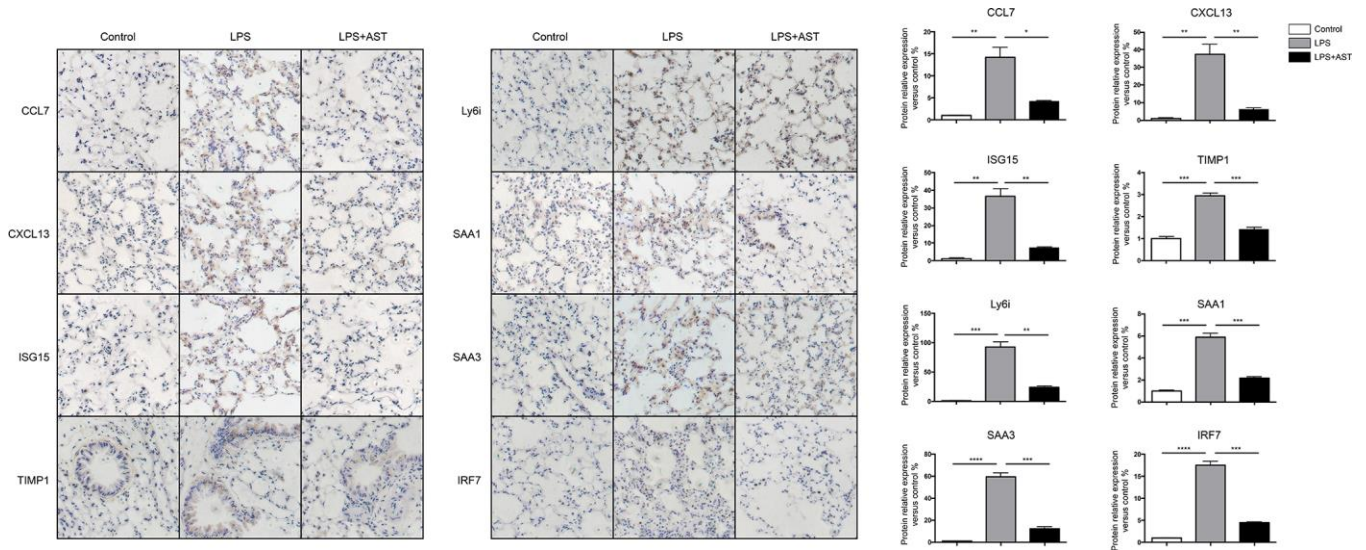
Supplementary Figure 4. Expression of the 8 core genes (*Ccl7, Saa3, Ly6i, Saa1, Irf7, Timp1, Isg15* and *Cxcl13*) determined by immunohistochemistry. Statistical analysis of the differences between groups was achieved with one-way ANOVA using Prism 7 software. ****p < 0.0001, ***p < 0.001, **p < 0.01, and *p < 0.05 were considered statistically significant.

Supplementary Tables

Please browse Full Text version to see the data of Supplementary Tables 1 to 3.

Supplementary Table 1. Characteristics of studies composing the LPS-induced ALI gene expression compendium.

Supplementary Table 2. Differentially expressed genes from the meta-analysis.

Supplementary Table 3. DEGs between LPS and control samples.

Supplementary Table 4. DEGs between AST and LPS samples.

Gene	sampleA	sampleB	baseMeanA	baseMeanB	baseMean	log2FoldChange	lfcSE	stat	pvalue	padj
ENSMUSG00000022818	AST	LPS	48.41487417	15.22940743	28.89401138	1.021436182	0.212138014	4.814960607	1.47229E-06	0.000673911
ENSMUSG00000059824	AST	LPS	569.0902514	204.3558614	354.5406102	1.022655966	0.202188092	5.057943611	4.23802E-07	0.000231532
ENSMUSG00000060600	AST	LPS	309.7794502	108.9422031	191.6398931	1.081034961	0.19750523	5.473449788	4.41358E-08	3.73742E-05
ENSMUSG00000048498	AST	LPS	342.5834924	70.69719237	182.6503747	1.167546697	0.218068915	5.354026256	8.60184E-08	6.62185E-05
ENSMUSG00000039109	AST	LPS	596.1148924	204.052468	365.4899369	1.167651944	0.188164286	6.205491853	5.45261E-10	9.23454E-07
ENSMUSG00000032915	AST	LPS	613.660102	149.1405857	340.4133277	1.183303614	0.21566635	5.486732691	4.09436E-08	3.73742E-05
ENSMUSG00000027338	AST	LPS	62.4055815	9.174534721	31.09320104	1.194972807	0.216388509	5.522348729	3.34498E-08	3.33238E-05
ENSMUSG00000033227	AST	LPS	19.33965891	1.81051473	9.028397628	1.433440935	0.217019981	6.605110399	3.97221E-11	1.34547E-07
ENSMUSG00000051682	AST	LPS	522.9979615	102.0594688	275.3870835	1.483269424	0.211237851	7.021797556	2.19032E-12	9.96623E-09

Supplementary Table 5. GO analysis of the 11 AST-associated genes.

ID	Description	BgRatio	pvalue	p.adjust	qvalue	geneID	Count
GO:0034364	high-density lipoprotein particle	23/23436	5.04E-05	0.000750507	0.000164585	20210/20208	2
GO:0034358	plasma lipoprotein particle	34/23436	0.000111442	0.000750507	0.000164585	20210/20208	2
GO:1990777	lipoprotein particle	34/23436	0.000111442	0.000750507	0.000164585	20210/20208	2
GO:0032994	protein-lipid complex	36/23436	0.000125085	0.000750507	0.000164585	20210/20208	2
GO:0020005	symbiont-containing vacuole membrane	12/23436	0.005619159	0.019216454	0.004214135	634650	1
GO:0020003	symbiont-containing vacuole	14/23436	0.006552889	0.019216454	0.004214135	634650	1
GO:0065010	extracellular membrane-bounded organelle	16/23436	0.007485823	0.019216454	0.004214135	634650	1
GO:0030430	host cell cytoplasm	17/23436	0.007951991	0.019216454	0.004214135	634650	1
GO:0033655	host cell cytoplasm part	17/23436	0.007951991	0.019216454	0.004214135	634650	1
GO:0033646	host intracellular part	20/23436	0.009349301	0.019216454	0.004214135	634650	1
GO:0043656	intracellular region of host	20/23436	0.009349301	0.019216454	0.004214135	634650	1
GO:0033643	host cell part	22/23436	0.010279847	0.019216454	0.004214135	634650	1
GO:0018995	host	24/23436	0.011209598	0.019216454	0.004214135	634650	1
GO:0043657	host cell	24/23436	0.011209598	0.019216454	0.004214135	634650	1
GO:0005881	cytoplasmic microtubule	78/23436	0.036014707	0.04801961	0.010530616	20208	1

Supplementary Table 6. The list of primer sequences used in this study.

1	GAPDH	forward	5′ -	AGGTCGGTGTGAACGGATTTG	- 3′
		reverse	5′ -	TGTAGACCATGTAGTTGAGGTCA	- 3′
2	Saa3	forward	5′ -	AGAGAGGCTGTTCAGAAGTTCA	- 3′
		reverse	5′ -	AGCAGGTCGGAAGTGGTTG	- 3′
3	Ly6i	forward	5′ -	CTGAGAGGAACCCTTCTCCAA	- 3′
		reverse	5′ -	GGTGTTCCACACACTACCCC	- 3′
4	Saa1	forward	5′ -	TGGCTGGAAAGATGGAGACAA	- 3′
		reverse	5′ -	AAAGCTCTCTCTTGCATCACTG	- 3′
5	Irf7	forward	5′ -	GAGACTGGCTATTGGGGGAG	- 3′
		reverse	5′ -	GACCGAAATGCTTCCAGGG	- 3′
6	Cxcl5	forward	5′ -	GTTCCATCTCGCCATTCATGC	- 3′
		reverse	5′ -	GCGGCTATGACTGAGGAAGG	- 3′
7	Ccl7	forward	5′ -	GCTGCTTTCAGCATCCAAGTG	- 3′
		reverse	5′ -	CCAGGGACACCGACTACTG	- 3′
8	Timp1	forward	5′ -	CGAGACCACCTTATACCAGCG	- 3′
		reverse	5′ -	ATGACTGGGGTGTAGGCGTA	- 3′
9	Isg15	forward	5′ -	AGTGATGCTAGTGGTACAGAACT	- 3′
		reverse	5′ -	CAGTCTGCGTCAGAAAGACCT	- 3′
10	Gbp11	forward	5′ -	CATTGCAGAGAAGTGCACCAA	- 3′
		reverse	5′ -	ATCACAGTCTCTCATTTGCTCC	- 3′
11	Tgtp1	forward	5′ -	TGGGACCACTAACTTCACACC	- 3′
		reverse	5′ -	GGCCAGTTGTGCATCATTTTC	- 3′
12	Cxcl13	forward	5′ -	GGCCACGGTATTCTGGAAGC	- 3′
		reverse	5′ -	GGGCGTAACTTGAATCCGATCTA	- 3′